Eur. Phys. J. D **6**, 133–143 (1999)

THE EUROPEAN PHYSICAL JOURNAL D

EDP Sciences

3D all optical local cooling in a bichromatic standing wave

W. Alge[a], K.M. Gheri, K. Ellinger, H. Stecher, and H. Ritsch

Institut für Theoretische Physik, Universität Innsbruck, Technikerstr. 25, 6020 Innsbruck, Austria

Received: 22 April 1998 / Received in final form: 5 November 1998

Abstract. We theoretically investigate an all optical scheme for three-dimensional trapping and cooling of atoms in a single bichromatic standing wave with a Gaussian transverse intensity profile as, *e.g.* formed by two different longitudinal modes of a linear optical cavity. The atoms are cooled through an efficient Sisyphus mechanism and trapped at those anti-nodes (maxima) of the stronger field where the second weaker field has a node. This generates a large effective atom-field coupling as it is desired in nonlinear optical experiments with clouds of atoms. The scheme effects high local densities modulated at the beat frequency of the two involved modes. In the appropriate parameter regime the results from a three-dimensional semi-classical approach are confirmed by a 1D full QMCWF-simulation. Extending our model to a more realistic case, we include loss channels out of the system and repumping. Furthermore, we generalise our approach to Λ-type level schemes, which exhibit promising optical nonlinearities. Trapping and cooling of such atoms is predicted to be compatible with maintaining high cooperativities needed for large nonlinear effects.

PACS. 32.80.Pj Optical cooling of atoms; trapping – 42.50.Vk Mechanical effects of light on atoms, molecules, electrons, and ions

1 Introduction

Since the successful introduction of the magneto-optical trap (MOT) samples of large numbers of very cold atoms have become a standard ingredient to numerous quantum optics experiments [1–4]. Recently, the well-defined and tailorable optical nonlinearities [5] of such atomic samples have been very successfully used in fundamental quantum optical experiments on optical bistability, generation of squeezed light [6] and in particular QND intensity measurements of optical beams [7]. Usually, the atoms at the center of a (dark-spot) MOT are strongly coupled to one or more focussed light beams or cavity fields whose quantum properties are modified through the interaction with the atoms. The atoms' centre-of-mass motion is substantially modified by these light fields and in general the atoms in the interaction region will be heated, *e.g.,* by dipole heating [8,9] so that the trap performance is strongly impaired. Although the effective size of the atom-field interaction region ($\approx$ 10–100 μm) is much smaller than the MOT-size (1–10 mm), dipole heating strongly limits the possible interaction times and field strengths. In this work, we propose a setup where by proper choice of detunings and field configuration (adding a second field) dipole heating is strongly reduced and even reversed into cooling [10]. This is accompanied by a periodic 3D confinement of the atoms around those anti-nodes (3D maxima) of the stronger field where the second weaker field is out of phase. Hence the atoms exhibit maximum atom-field coupling as desired, but are hardly influenced by the second field.

In addition, due to the mismatch of the two wave vectors this long-range density modulation greatly enhances the local density at the trapping points. Hence our system, which could be realized using the D1 and D2 line of alkalis should find application in many nonlinear optics experiments based on cold atoms coupled to cavity fields. In particular, it could be successfully used to trap one or a few atoms in a high-Q optical micro-cavity [11,12]. This would provide large atom field coupling throughout a sufficiently long period of time. Here only two (quasi-1D) intra-cavity modes are required to achieve 3D confinement, which would greatly simplify the experimental effort involved.

The most promising systems known to exhibit large nonlinear optical effects are atoms with a Λ level scheme interacting with a very strong and a weaker light field. The most relevant parameter regime is where the weaker field is tuned to the vicinity of the Autler-Townes Doublet [13] caused by the stronger field. This scheme was used by Roch, Grangier and coworkers for their recent breakthrough in QND measurements [7]. It is particularly interesting whether the forces induced by the light fields tend to increase or decrease the cooperativity in such a setup. Therefore, we also investigate trapping and cooling in 3D for a Λ-system. For suitable parameters the trapping efficiency is almost as large as for the scheme proposed by us. Moreover, the most interesting results occur in the most relevant parameter regime mentioned above.

[a] e-mail: `wieland.alge@uibk.ac.at`

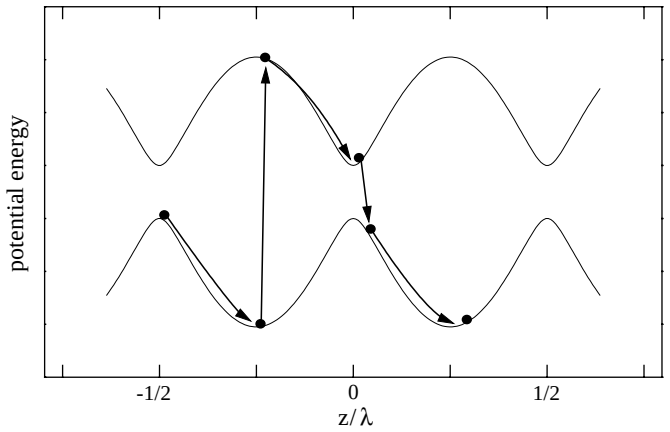

Fig. 1. The typical motion in the adiabatic potentials seen by a slowly moving two-level atom in a standing wave with parameters $\Omega = 5\Delta$.

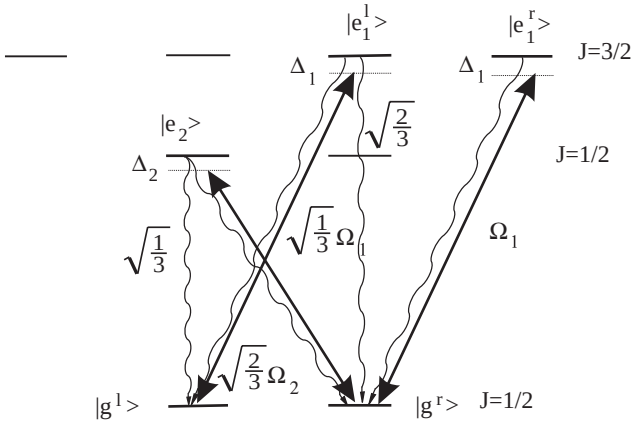

Fig. 2. Energy levels and transitions involved. A strong σ_+-polarized laser dresses the $\frac{1}{2} - \frac{3}{2}$ transition. The weaker σ_--polarized laser leads to a spatially dependent redistribution of the populations of the adiabatic potentials created by the stronger one.

This work is organised as follows. First we briefly review the light-induced forces acting on a two-level atom in a strong standing wave. Then we present an overview of the mathematical methods and approximations used at the example of the XV-system. The validity of the semi-classical approach is confirmed through a comparison with a full Quantum Monte Carlo wave function simulation (in 1D). Finally the main results of the semi-classical simulations in three dimensions are discussed. This part concludes with an extension of our model to open transitions which is a well known experimental situation. The next part of the paper deals with the mechanical light effects in a generic Λ level configuration. Again we discuss qualitatively the underlying physical mechanisms and conclude with a discussion of the three-dimensional results.

2 Atoms in strong standing waves

2.1 Two-level atom

The mechanical light effects present in the simple configuration of a two-level atom moving in a strong 1D standing wave are well known and have been extensively discussed in a seminal paper by Dalibard and Cohen-Tannoudji [14]. Let us deal with the case of very strong fields where the secular approximation is valid which allows us to neglect the coherences between the adiabatic eigenstates (Thomas-Fermi approximation) of the Hamiltonian. Then the ponderomotive effect experienced by a moderately slowly moving atom is an "up and down" in the adiabatic potentials formed by the eigenvalues of the internal Hamiltonian at each point. The contribution from the excited level to the local eigenstates determines the probability to change the potential. Figure 1 depicts the potentials for the case of red detuning and shows the most probable way of moving within them. From this figure it can be seen that red detuning leads to a Sisyphus heating mechanism which expels the atoms from the regions of maximum interaction. Blue detuning has the disadvantage that the atoms tend to be localized around the nodes of the field so that they are easily lost in radial direction. That is why it is rather difficult to investigate nonlinear optical effects with strong standing waves. In the next section we propose a scheme that holds the promise to overcome the sketched problems.

2.2 Multilevel systems

As the simplest nontrivial example we consider an atom with two ground states and three excited states as depicted in Figure 2. This model contains all the essential physics and at the same time permits a numerical solution within a reasonable amount of time. Note that we take all relevant levels of the $J = \frac{1}{2}$ ground and $J = \frac{1}{2}, \frac{3}{2}$ upper manifolds. The results should also apply to higher angular-momentum transitions of the type $J \to J, J \to J + 1$, in particular to the configuration used in a recent experiment by Grangier and coworkers [7], who use $2 \to 2$ and $2 \to 3$ transitions within the D_1- and D_2-line of rubidium.

The two standing waves are modeled as classical monochromatic light fields. The stronger one is σ_+-polarized and acts on the $\frac{1}{2} \to \frac{3}{2}$ transition, whereas the weaker one is σ_--polarized and acts on the $\frac{1}{2} \to \frac{1}{2}$ transition. If this second laser is turned off, the atom will simply behave as a two-level system because of optical pumping and the atom will soon be expelled from the interaction zone with the laser field through dipole heating [14,15]. The relevant transitions along with their Clebsch-Gordan coefficients and the applied light fields are shown in Figure 2. The Hilbert-space of the system is given by

$$\mathcal{H} = \mathbf{C}^5 \otimes L^2(\mathbf{R}^s)\,,$$

where s is the spatial dimension of the configuration space (1D or 3D). As a major generalization of many previous discussions of similar systems, we do not limit ourselves to parameter regimes where an adiabatic elimination of

the excited states is justified, since we are interested in the case of strong atom-field coupling. A Hamiltonian accounting for the free kinetic, the free internal part and the interaction energy reads

$$H = \frac{P^2}{2m} - \sum_{i=1,2} \Delta_i \Pi_{e_i} + \frac{\Omega_1(x)}{2}(A_+ + A_+^\dagger) + \frac{\Omega_2(x)}{2}(B_- + B_-^\dagger)\,, \tag{1}$$

where $\Omega_i(\mathbf{x})$ is the position dependent Rabi frequency of the i-th light field and $\Delta_i = \omega_i - (E_{e_i} - E_g)$ the detuning from the atomic transition $g - e_i$. Π_{e_i} is the projection operator on the i-th excited level subspace. The operator A_+ is the annihilation operator of the $g - e_1$ transition and B_- of the $g - e_2$ transition, respectively, including the Clebsch-Gordan coefficients [16]:

$$A_+ = \frac{1}{\sqrt{3}}|g^{\mathrm{l}}\rangle\langle e_1^{\mathrm{l}}| + |g^{\mathrm{r}}\rangle\langle e_1^{\mathrm{r}}|\,, \qquad A_0 = \sqrt{\frac{2}{3}}|g^{\mathrm{r}}\rangle\langle e_1^{\mathrm{l}}|\,,$$
$$B_- = \sqrt{\frac{2}{3}}|g^{\mathrm{r}}\rangle\langle e_2|\,, \qquad B_0 = -\frac{1}{\sqrt{3}}|g^{\mathrm{l}}\rangle\langle e_2|\,.$$

The density operator ρ fulfils the following master equation of Lindblad type [17]:

$$\dot\rho = -i(H_{\mathrm{eff}}\rho - \rho H_{\mathrm{eff}}^\dagger) + \mathcal{J}\rho \tag{2}$$

with

$$H_{\mathrm{eff}} = H - \frac{i}{2}(\Gamma_1\Pi_{e_1} + \Gamma_2\Pi_{e_2})\,,$$
$$\mathcal{J}\rho = \frac{3\Gamma_1}{8\pi}\sum_{\sigma,\sigma'}\int \mathrm{d}\Omega_{\mathbf{n}} N_{\sigma\sigma'}(\mathbf{n}) e^{-ik_1\mathbf{n}\cdot\mathbf{x}} A_\sigma \rho A_{\sigma'}^\dagger e^{ik_1\mathbf{n}\cdot\mathbf{x}} + \frac{3\Gamma_2}{8\pi}\sum_{\sigma,\sigma'}\int \mathrm{d}\Omega_{\mathbf{n}} N_{\sigma\sigma'}(\mathbf{n}) e^{-ik_2\mathbf{n}\cdot\mathbf{x}} B_\sigma \rho B_{\sigma'}^\dagger e^{ik_2\mathbf{n}\cdot\mathbf{x}}\,,$$

where $N_{\sigma\sigma'}(\mathbf{n}) = \delta_{\sigma\sigma'} - (\mathbf{e}_\sigma\cdot\mathbf{n})(\mathbf{e}_{\sigma'}\cdot\mathbf{n})$ is the polarization-dependent spatial distribution of the fluorescent photons with $\mathbf{n}$ being a unit vector and Γ_i the full natural linewidths of the excited states $|e_i\rangle$.

In order to treat 3D confinement, we choose a semiclassical approach and study the evolution of the Wigner operator $W(\mathbf{x},\mathbf{p},t)$ of the atom:

$$W(\mathbf{x},\mathbf{p},t) = \int \frac{\mathrm{d}^3u}{\pi^3}\langle\mathbf{p}+\mathbf{u}|\rho(t)|\mathbf{p}-\mathbf{u}\rangle e^{i2\mathbf{u}\cdot\mathbf{x}}\,.$$

Under the assumption that $\hbar k$ is much smaller than the typical variation of the Wigner operator $W(\mathbf{x},\mathbf{p},t)$ on the momentum subspace one can transform the master equation (2) into a Fokker-Planck–type operator equation

$$\frac{\partial}{\partial t}W(\mathbf{x},\mathbf{p},t) + \frac{\mathbf{p}}{m}\cdot\nabla_x W(\mathbf{x},\mathbf{p},t) = \left(\mathcal{L}^{(0)} + \mathcal{L}^{(1)} + \mathcal{L}^{(2)}\right) W(\mathbf{x},\mathbf{p},t)\,, \tag{3}$$

where $\mathcal{L}^{(\alpha)}(\alpha = 0,1,2)$ denotes the operator of order α in the $\hbar k$-expansion [18,19].

The internal Hilbert space separates into two coherently decoupled parts, one spanned by $\{|g^{\mathrm{l}}\rangle, |e_1^{\mathrm{l}}\rangle\}$ and the other one by $\{|g^{\mathrm{r}}\rangle, |e_1^{\mathrm{r}}\rangle, |e_2\rangle\}$, respectively. Within these subsets the eigenvalues of the Hamiltonian are well separated for our parameters ($\Omega, \Delta \gg \Gamma$). Hence we may make use of a secular approximation and neglect the off-diagonal part of the density operator. Equation (3) is rewritten in the basis of the eigenstates of the internal Hamiltonian (dressed states). We obtain a system of five coupled Fokker-Planck–type equations for the populations of the atomic dressed states [20]. We want to mention that for the systems treated in this work only positive diffusion coefficients (this is not the case in [20]) occur which is a necessary prerequisite for the use of a Monte Carlo technique.

Since the adiabatic potentials are rather steep, the acceleration of the atoms can be large and their internal degrees of freedom may not be adiabatically eliminated ("oscillation regime" [21]). The motion of an atom in the two standing waves is hence determined by a multi-potential motion in the adiabatic potentials interrupted by jumps from one well into another, with a recoil kick into a random direction. The intermediate adiabatic motion is numerically evaluated using a stochastic modified midpoint method which is equivalent to a stochastic fourth-order Runge-Kutta method. In order to limit the necessary computation time, we have to avoid a numerical calculation of the eigenvectors in each step of the time propagation. As the exact analytic expressions of the dressed states are rather involved, we employ the following approximation, which is discussed in more detail for the similar case of the Λ configuration in the appendix.

First we calculate the dressed states for the case when there is no σ_--field. This yields a set of states which we choose to label $|+_{\mathrm{l}}\rangle, |-_{\mathrm{l}}\rangle, |+_{\mathrm{r}}\rangle, |-_{\mathrm{r}}\rangle, |e_2\rangle$ with

$$|+_{\mathrm{l}}\rangle = \cos\theta_{\mathrm{l}}|e_1^{\mathrm{l}}\rangle + \sin\theta_{\mathrm{l}}|g^{\mathrm{l}}\rangle\,, \tag{4}$$
$$|-_{\mathrm{l}}\rangle = -\sin\theta_{\mathrm{l}}|e_1^{\mathrm{l}}\rangle + \cos\theta_{\mathrm{l}}|g^{\mathrm{l}}\rangle\,, \tag{5}$$
$$|+_{\mathrm{r}}\rangle = \cos\theta_{\mathrm{r}}|e_1^{\mathrm{r}}\rangle + \sin\theta_{\mathrm{r}}|g^{\mathrm{r}}\rangle\,, \tag{6}$$
$$|-_{\mathrm{r}}\rangle = -\sin\theta_{\mathrm{r}}|e_1^{\mathrm{r}}\rangle + \cos\theta_{\mathrm{r}}|g^{\mathrm{r}}\rangle\,, \tag{7}$$
$$\cos 2\theta_{\mathrm{l}} = \frac{-\Delta_1}{\sqrt{\Delta_1^2 + \frac{1}{3}\Omega_1^2}}\,, \tag{8}$$
$$\sin 2\theta_{\mathrm{l}} = \frac{\sqrt{\frac{1}{3}}\Omega_1}{\sqrt{\Delta_1^2 + \frac{1}{3}\Omega_1^2}}\,, \tag{9}$$
$$\cos 2\theta_{\mathrm{r}} = \frac{-\Delta_1}{\sqrt{\Delta_1^2 + \Omega_1^2}}\,, \tag{10}$$
$$\sin 2\theta_{\mathrm{r}} = \frac{\Omega_1}{\sqrt{\Delta_1^2 + \Omega_1^2}}\,. \tag{11}$$

Then we assume that the detuning of the σ_--polarised field is chosen to be nearly resonant with ($|+_{\mathrm{r}}\rangle$ or $|-_{\mathrm{r}}\rangle$). We treat the resonant level together with the excited level $|e_2\rangle$ of the second transition as a driven two-level system

and calculate the dressed states of this subsystem. Now if the σ_--laser is detuned to the lower Rabi-level $|-_{\rm r}\rangle$ we end up with the basis $|+_{\rm l}\rangle, |-_{\rm l}\rangle, |+_{\rm r}\rangle, |a\rangle, |b\rangle$ with their approximate energies $E^{\rm l}_+, E^{\rm l}_-, E^{\rm r}_+, E_a, E_b$:

$$|a\rangle = \cos\phi|e_2\rangle - \sin\phi\sin\theta_{\rm r}|e^{\rm r}_1\rangle + \sin\phi\cos\theta_{\rm r}|g^{\rm r}\rangle\,, \quad (12)$$

$$|b\rangle = -\sin\phi|e_2\rangle - \cos\phi\sin\theta_{\rm r}|e^{\rm r}_1\rangle + \cos\phi\cos\theta_{\rm r}|g^{\rm r}\rangle\,, \quad (13)$$

$$E_a = -\frac{\Delta_2 + \sqrt{\Delta_1^2+\Omega_1^2}\sin^2\theta_{\rm r}}{2} + \frac{E_2}{2}\,, \quad (14)$$

$$E_b = -\frac{\Delta_2 + \sqrt{\Delta_1^2+\Omega_1^2}\sin^2\theta_{\rm r}}{2} - \frac{E_2}{2}\,, \quad (15)$$

$$\cos 2\phi = \frac{-(\Delta_2 - \sqrt{\Delta_1^2+\Omega_1^2}\sin^2\theta_{\rm r})}{E_2}\,, \quad (16)$$

$$\sin 2\phi = \frac{\Omega_2\cos\theta_{\rm r}}{E_2}\,, \quad (17)$$

$$E_2 = \sqrt{(-\Delta_2 + \sqrt{\Delta_1^2+\Omega_1^2}\sin^2\theta_{\rm r})^2 + \Omega_2^2\cos^2\theta_{\rm r}}\,. \quad (18)$$

$|a\rangle, |b\rangle$ are linear combinations of each of the three levels $|g^{\rm r}\rangle, |e^{\rm r}_1\rangle, |e_2\rangle$ which together form a V scheme.

This provides an excellent and robust approximation for a large range of parameters [22]. For typical parameters used in the simulations the error incurred by the approximation is at most of the order of one percent.

3 Local sisyphus cooling with the XV system

3.1 Qualitative treatment

Parameters yielding interesting results can be realized experimentally by choosing the D_1- and D_2-line of rubidium. (For rubidium the Doppler limit for the width of the momentum distribution is $28\hbar k$ on the D_1-line. The recoil frequency $\omega_{\rm R}$ is $3.7 \times 2\pi$kHz.) This setup is similar to the one used by Grangier and coworkers for QND-measurements [7].

The most interesting parameter regime results can be found from the following considerations. In order to avoid radial diffusion and to trap the atoms at spatial regions with high field intensity the strong laser should be red detuned. To avoid the dominant dipole heating, its detuning has to be large enough that the population of the upper dressed levels is reasonably small. The second weaker standing wave should act as a repumper between the two lower highly populated dressed levels in a way that a local Sisyphus mechanism is established. It turns out that the best results are achieved, if it is tuned to the blue side of the lower dressed level (*i.e.* below it in Fig. 3).

To get a feel for the mechanism at work we have a look at the adiabatic potentials seen by a slowly moving atom and their steady-state populations [23]. Almost all (more than 99%) atoms are in the states $|-_{\rm l}\rangle$ and $|a\rangle$. The lower dressed state of the $|g^{\rm l}\rangle - |e^{\rm l}_1\rangle$ transition is $|-_{\rm l}\rangle$ and $|a\rangle$ is the upper state resulting from dressing the lower dressed state of the $|g^{\rm r}\rangle - |e^{\rm r}_1\rangle$ transition with the second weaker

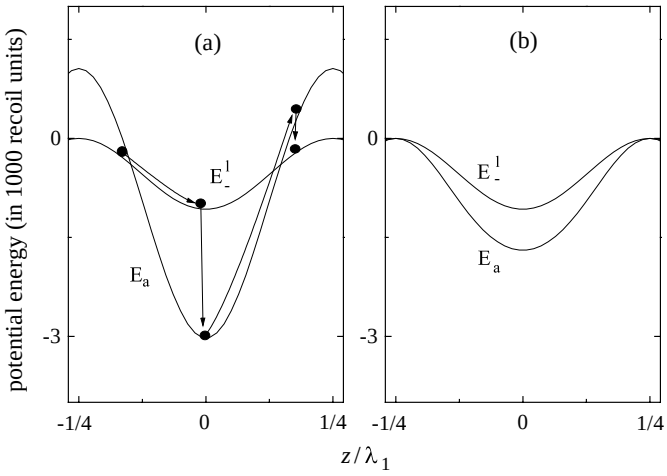

Fig. 3. The highly populated adiabatic potentials. The left plot shows the case of the standing waves having a relative phase difference of $\pi/2$ whereas in the right plot they are in phase. The length of the ordinate is slightly more than half a wavelength. The parameters are $\Omega_1 = 13.3\Gamma_1$, $\Delta_1 = -20\Gamma_1$, $\Gamma_1 = 1500\,\omega_{\rm R}$; $\Omega_2 = 5.3\Gamma_2$, $\Delta_2 = 6\Gamma_2$, $\Gamma_2 = \Gamma_1$.

field. The two potentials of these states are depicted in Figure 3. The right one shows the situation where the two light-fields are in phase. There the depth of the potential induced by the strong σ_+- field is reduced (without the second field it would be three times as deep as the shallow one due to a larger Clebsch-Gordan coefficient, cf. Fig. 2). The σ_+-polarized field pumps the atoms from the $|-_{\rm l}\rangle$ state to the $|a\rangle$ state whereas the σ_--polarized field does just the opposite. When the two light fields are in phase, these two processes tend to cancel each other. Hence the populations do not vary much along one wavelength (Fig. 4).

The situation is completely different when the two fields have a phase difference of $\pi/2$ (Fig. 3a). There the deeper potential is shifted towards positive energies at the nodes of the σ_+ field and gets steeper than without the presence of the σ_- light field. Furthermore, the two pumping processes have spatially distinguished regions of efficiency. Therefore all steady-state population at the antinodes of the first light field is in the deeper potential whereas at the nodes all atoms are in the flat one (Fig. 5). For a slowly moving atom this leads to an efficient local Sisyphus effect. A typical path of an atom in these potentials is sketched in Figure 3a. We want to emphasize again that the states $|-_{\rm l}\rangle$ and $|a\rangle$ belong to two disjoint subsets of the Hilbert space and are coherently decoupled. Hence the crossing of the energy levels in Figure 3 does not create coherences between the states and does not allow nonadiabatic transitions from one level to the other.

3.2 1D semiclassical and Quantum Monte Carlo simulations

In order to develop a qualitative understanding and also to test the validity and limitations of this method we first

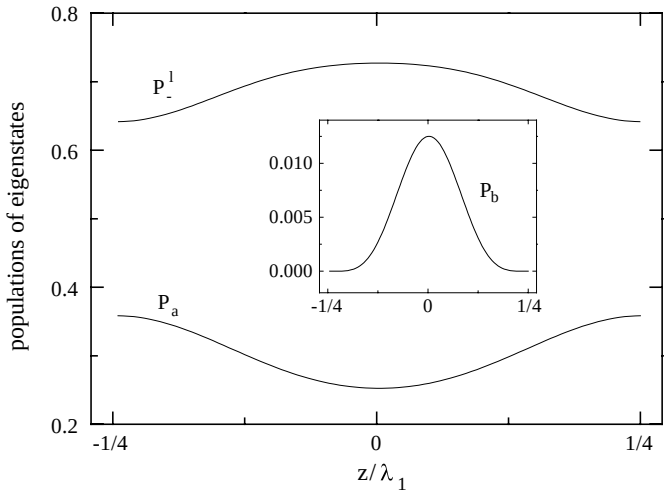

Fig. 4. Stationary population of adiabatic potentials as a function of position for a standing wave with no relative phase difference. The parameters are $\Omega_1 = 13.3\Gamma_1,\ \Delta_1 = -20\Gamma_1,\ \Gamma_1 = 1500\,\omega_{\rm R};\ \Omega_2 = 5.3\Gamma_2,\ \Delta_2 = 6\Gamma_2,\ \Gamma_2 = \Gamma_1$.

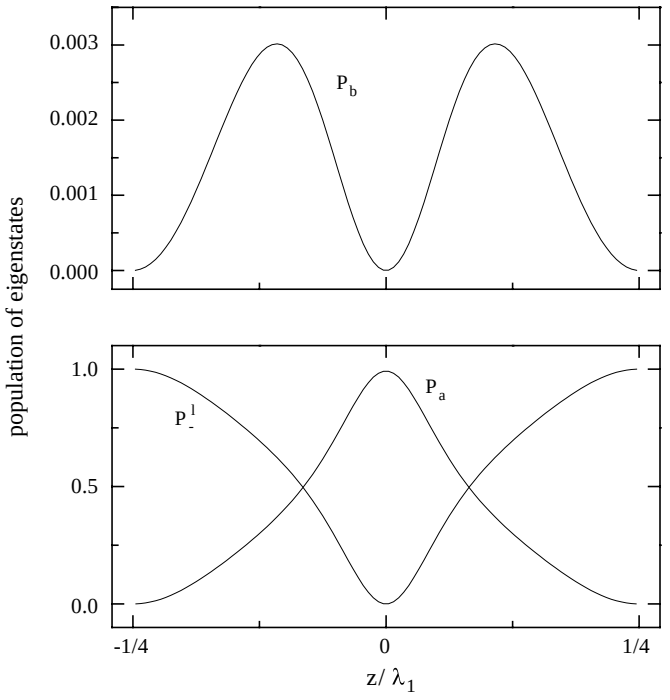

Fig. 5. Same as Figure 4 but for a relative phase difference of $\pi/2$.

limit ourselves to the 1D case, where a direct full Quantum Monte Carlo wave function (QMCWF) simulation [24,25] and thus a comparison are feasible.

The results of the semiclassical simulations reflect the expectations outlined in the preceding paragraphs. The atoms are trapped at those locations in the superlattice where the two light fields have a phase difference of $\frac{\pi}{2}$ with a momentum distribution having a width of the order of 10–15 $\hbar k$. For rubidium this is in the sub-Doppler regime.

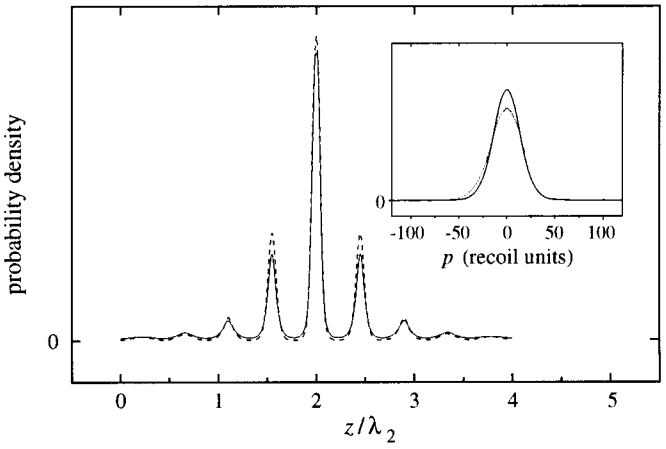

Fig. 6. Comparison of the spatial and momentum distributions obtained from a semi-classical simulation (dotted) with the ones from a Quantum Monte Carlo simulation (solid line). The parameters are $\Omega_1 = 13.3\Gamma_1,\ \Delta_1 = -40\Gamma_1,\ \Gamma_1 = 1500\,\omega_{\rm R};\ \Omega_2 = 2\Gamma_2,\ \Delta_2 = 6\Gamma_2,\ \Gamma_2 = \Gamma_1;\ k_1 = 1.125 \times k_2$.

Figure 6 depicts the spatial and the momentum distribution for the same parameters obtained by semi-classical and QMCWF simulation techniques. The agreement of the two approaches is excellent and confirms the validity of the semiclassical approach. In the QMCWF simulation the excited levels of the atoms have been adiabatically eliminated and therefore the model does not include dipole heating. This is why the momentum distribution obtained from the QMCWF simulation is slightly narrower than the semiclassical results. The Rabi frequencies are $\Omega_i(z) = \Omega_i \sin k_i z$.

The main goal of this comparison is to test the validity of the semiclassical description of the atomic motion. The reliability of the secular approximation, however, should even improve with increasing strength of the light fields which is the case we will be considering in the three-dimensional model.

4 3D cooling and trapping in a Gaussian wave field

In a real 3D configuration as, *e.g.*, a cavity mode, the light fields in radial direction can be modeled by a simple Gaussian distribution($\Omega_i(\mathbf{x}) = \Omega_i \sin(k_i z) \exp(-m_i(x^2+y^2))$). A potential problem of trapping atoms in 3D with the configuration used in 1D before is the repelling potential of the blue detuned second laser seen by the atoms at the nodes of the strong laser. Fortunately, the trapping mechanism is so strong that the atoms are hardly ever at these critical points and if so, they are slow enough that the population is likely to be pumped to the state $|g^1\rangle$ which does not couple to the blue laser. So it turns out that the dominant escape mechanism is only that of accumulating random momentum kicks in the radial direction (radial diffusion). The potentials, however, are steep enough to trap the atoms long enough to use them for nonlinear optical experiments.

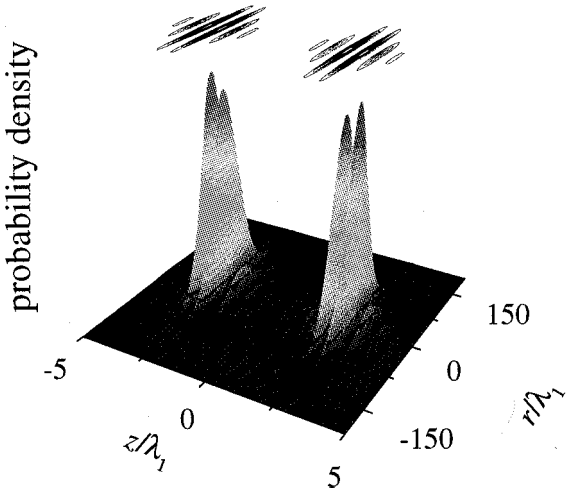

Fig. 7. Spatial distribution of the atoms over one period of the super-lattice. The z-axis is the direction of the two light fields. The parameters are $\Omega_1 = 13.3\Gamma_1$, $\Delta_1 = -20\Gamma_1$, $\Gamma_1 = 1500\,\omega_\mathrm{R}$; $\Omega_2 = 4\Gamma_2$, $\Delta_2 = 5.3\Gamma_2$, $\Gamma_2 = \Gamma_1$; $k_2 = 0.9 \times k_1$. The FWHM of the light fields in radial direction is $140/k_1$. The explicit spatial dependence of the two standing waves is $\Omega_i(\mathbf{x}) = \Omega_i \sin(k_i z) \exp(-m_i(x^2 + y^2))$.

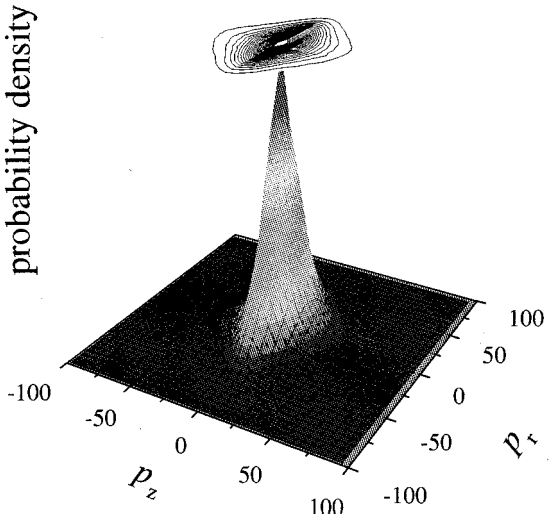

Fig. 8. Momentum distribution of the atoms. The z-axis is the direction of the two light fields. The parameters are $\Omega_1 = 13.3\Gamma_1$, $\Delta_1 = -20\Gamma_1$, $\Gamma_1 = 1500\,\omega_\mathrm{R}$; $\Omega_2 = 4\Gamma_2$, $\Delta_2 = 5.3\Gamma_2$, $\Gamma_2 = \Gamma_1$; $k_2 = 0.9 \times k_1$. The FWHM of the light fields in radial direction is $140/k_1$.

Figure 7 shows the spatial distribution of the atoms and the momentum distribution. The z-axis is the laser direction. From the momentum distribution (Fig. 8) one can see that the cooling in longitudinal direction is excellent (the FWHM is about 10 $\hbar k_1$) while the radial momentum spread is substantially larger (the FWHM is about 30 $\hbar k_1$), but still narrow enough to strongly limit the transverse trap loss rate. The resulting spatial distribution shows that the atoms are strongly confined within the superlattice at the regions, where the two standing waves have a phase shift of $\pi/2$ and the strong light field has its maxima. Hence we can expect high local densities and large cooperativities even for fairly small numbers of atoms as they will not be smeared out evenly over the whole interaction volume.

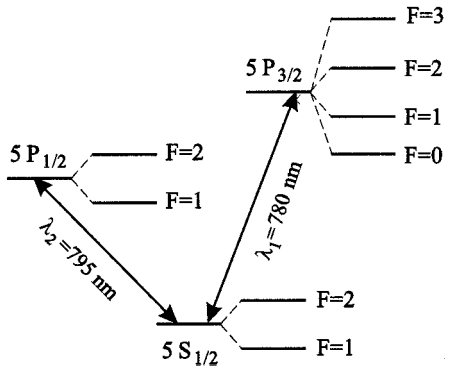

Fig. 9. The level scheme of the hyperfine structure of the D_1 and D_2 line of ^{87}Rb.

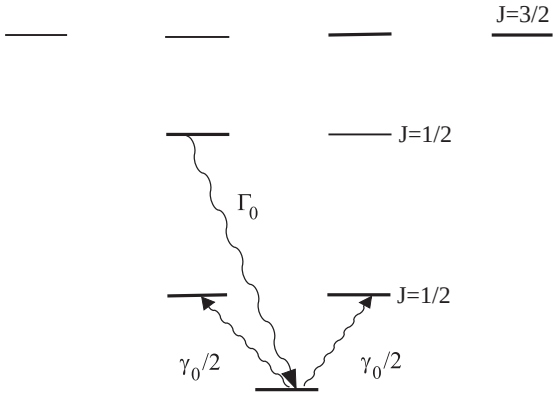

Fig. 10. The level scheme of the extended model with an additional spectator level and the rates which affect the population of it.

4.1 Hyperfine structure and repumping

For a practical realisation of this cooling scheme in alkali atoms the assumption of closed transitions has to be thought over. This assumption is valid only in our $\frac{1}{2} \rightarrow \frac{3}{2}, \frac{1}{2} \rightarrow \frac{1}{2}$ configuration. For example in ^{87}Rb the only closed transition for the σ_+-wave is a $2 \rightarrow 3$ transition, but then the $2 \rightarrow 2$ transition of the σ_--wave is not closed (see Fig. 9). To model this we add a so-called *spectator level* which the level $|e_2\rangle$ can decay into with a rate Γ_0. This level is practically decoupled from the standing waves and is repumped to one of the ground levels $|g_\mathrm{l}\rangle, |g_\mathrm{r}\rangle$ with a certain rate γ_0. This can be achieved for example by applying a diode-laser from the side. Figure 10 depicts the extension of the level scheme sketched in Figure 2.

Figures 11 and 12 depict the effects of the inclusion of a spectator level with reasonable pump rates in and out of it. As one can see, the radial width of the spatial distribution is increased and therefore also the probability for an atom to leave the radial focus. Nevertheless the effect is too

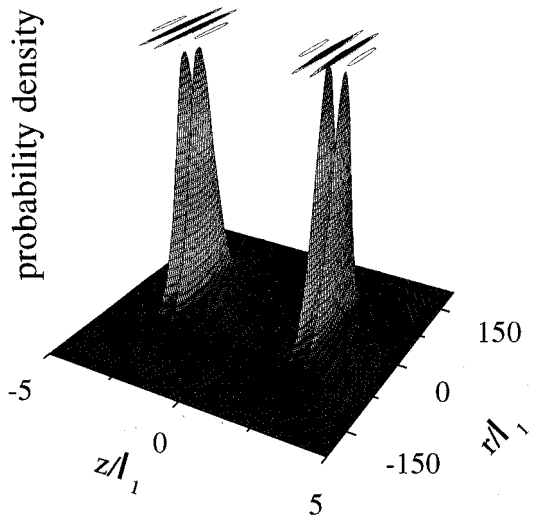

Fig. 11. Spatial distribution of the atoms over one period of the super-lattice. The z-axis is the direction of the two light fields. The parameters are $\Omega_1 = 13.3\Gamma_1$, $\Delta_1 = -20\Gamma_1$, $\Gamma_1 = 1500\,\omega_{\rm R}$; $\Omega_2 = 4\Gamma_2$, $\Delta_2 = 5.3\Gamma_2$, $\Gamma_2 = \Gamma_1$; $k_2 = 0.9\times k_1$, $\Gamma_0 = \Gamma_2/3$, $\gamma_0 = \Gamma_0/5$. The FWHM of the light fields in radial direction is $140/k_1$. The explicit spatial dependence of the two standing waves is $\Omega_i(\mathbf{x}) = \Omega_i \sin(k_i z)\exp(-m_i(x^2+y^2))$.

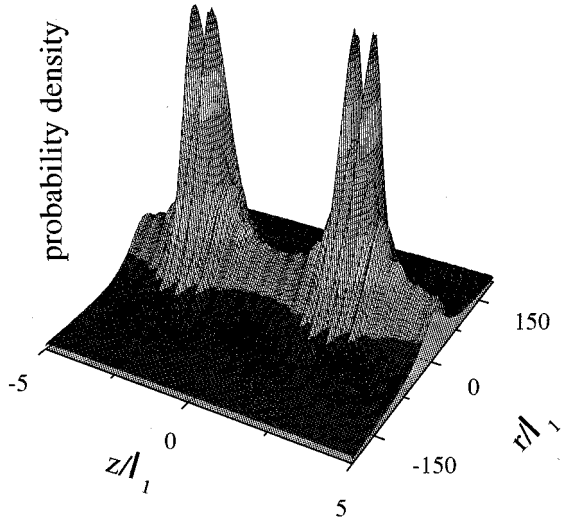

Fig. 13. Spatial distribution of the atoms over one period of the super-lattice. The z-axis is the direction of the two light fields. The parameters are $\Omega_1 = 13.3\Gamma_1$, $\Delta_1 = -20\Gamma_1$, $\Gamma_1 = 1500\,\omega_{\rm R}$; $\Omega_2 = 4\Gamma_2$, $\Delta_2 = 5.3\Gamma_2$, $\Gamma_2 = \Gamma_1$; $k_2 = 0.9\times k_1$, $\Gamma_0 = \Gamma_2/3$, $\gamma_0 = \Gamma_0/100$. The FWHM of the light fields in radial direction is $140/k_1$. The explicit spatial dependence of the two standing waves is $\Omega_i(\mathbf{x}) = \Omega_i \sin(k_i z)\exp(-m_i(x^2+y^2))$.

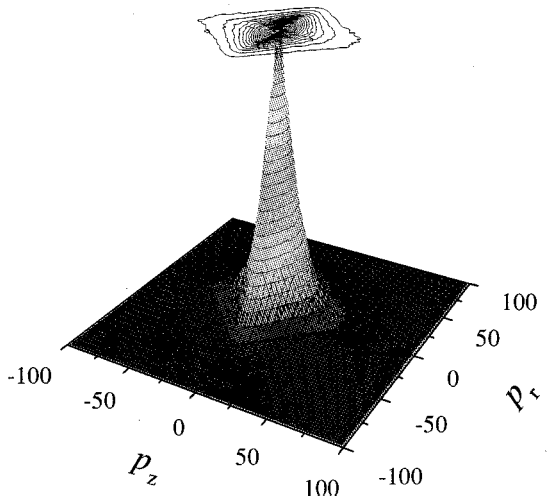

Fig. 12. Momentum distribution of the atoms. The z-axis is the direction of the two light fields. The parameters are $\Omega_1 = 13.3\Gamma_1$, $\Delta_1 = -20\Gamma_1$, $\Gamma_1 = 1500\,\omega_{\rm R}$; $\Omega_2 = 4\Gamma_2$, $\Delta_2 = 5.3\Gamma_2$, $\Gamma_2 = \Gamma_1$; $k_2 = 0.9\times k_1$, $\Gamma_0 = \Gamma_2/3$, $\gamma_0 = \Gamma_0/5$. The FWHM of the light fields in radial direction is $140/k_1$.

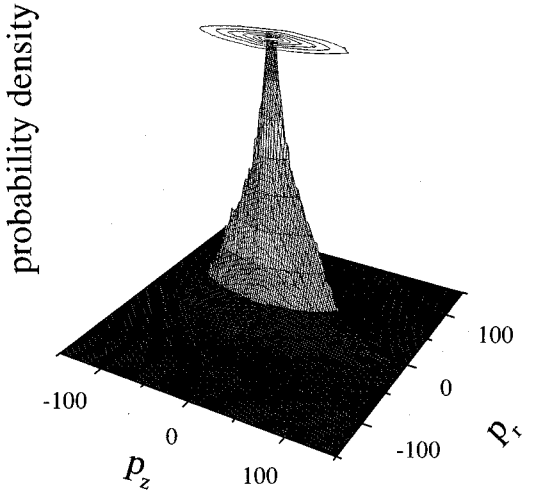

Fig. 14. Momentum distribution of the atoms. The z-axis is the direction of the two light fields. The parameters are $\Omega_1 = 13.3\Gamma_1$, $\Delta_1 = -20\Gamma_1$, $\Gamma_1 = 1500\omega_{\rm R}$; $\Omega_2 = 4\Gamma_2$, $\Delta_2 = 5.3\Gamma_2$, $\Gamma_2 = \Gamma_1$; $k_2 = 0.9\times k_1$, $\Gamma_0 = \Gamma_2/3$, $\gamma_0 = \Gamma_0/100$. The FWHM of the light fields in radial direction is $140/k_1$.

small to substantially modify the cooling mechanism for fast enough pumping.

If, however, the strength of the repumper is substantially smaller, many atoms will leave the regions where the cooling and trapping mechanism works and will be heated. Figures 13 and 14 depict the effects of a too small repumping rate. The longitudinal width of the momentum distribution is much larger than in Figure 12 which is caused by the fact that the atoms are no longer confined at the out-of-phase regions of the two standing waves. The radial width of the spatial distribution is substantially increased, which diminishes the time an atom is bound to the centre of the Gaussian mode.

5 Atoms with a bichromatic Lambda scheme

As already mentioned, the most promising system to exhibit strong nonlinear optical effects with low noise are atoms with a Lambda level configuration interacting with a strong and a weaker light field [5,22]. In the following section we investigate the mechanical effects present for

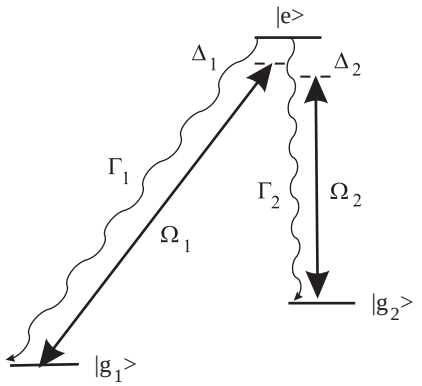

Fig. 15. Energy levels and transitions involved.

such a setup where the two light fields are realized by two different longitudinal TEM_{00} Gaussian modes in a cavity. Again we are able to find parameters where the atoms are pushed to the anti-nodes of the light field and are cooled down to reasonably small temperatures. For rubidium the temperatures are of the order of the Doppler limit, but in a parameter regime where the dipole heating would shift the minimum temperature achievable for a two-level system far above the optimum Doppler limit for a two-level atom. By comparison with the XV system the trapping efficiency is smaller but the atoms accumulate where both waves have their maximum. This is crucial for obtaining a substantial nonlinear interaction between the two light fields. It is exactly this feature which one needs to perform experiments which aim at achieving strong nonlinear interaction between two light fields.

5.1 The model

Like the XV system we study the Λ in a superlattice formed by two collinear standing waves of different frequencies as depicted in Figure 15.

The Hamiltonian of the atom in the rotating frame using dipole and rotating-wave approximation reads:

$$H = \frac{P^2}{2m} + \sum_{i=1,2} \Delta_i \Pi_{g_i} + \frac{\Omega_1(x)}{2}(\sigma_1 + \sigma_1^\dagger) + \frac{\Omega_2(x)}{2}(\sigma_1 + \sigma_1^\dagger)\,, \tag{19}$$

where $\Omega_i(\mathbf{x}) = \Omega_i \sin(k_i z)\exp(-m_i(x^2+y^2))$ is the position-dependent Rabi frequency of the i-th light field and $\Delta_i = \omega_i - (E_e - E_{g_i})$ the detuning from the atomic transition $g_i - e$. Π_{g_i} is the projection operator on the i-th ground level subspace. The operator $\sigma_1(\sigma_2)$ is the annihilation operators of the $g_1 - e(g_2 - e)$ transition. We choose the polarisation of the first transition to be σ_+ and that of the second one to be σ_-.

All further steps to obtain numerically soluble equations are analogous to the ones described in the preceding section. We diagonalize the internal Hamiltonian of the atom in the same way as discussed for the V system and use a $\hbar k$ expansion of the time evolution equation for the Wigner operator in the new basis neglecting all coherences. Details of the diagonalisation can be found in the appendix.

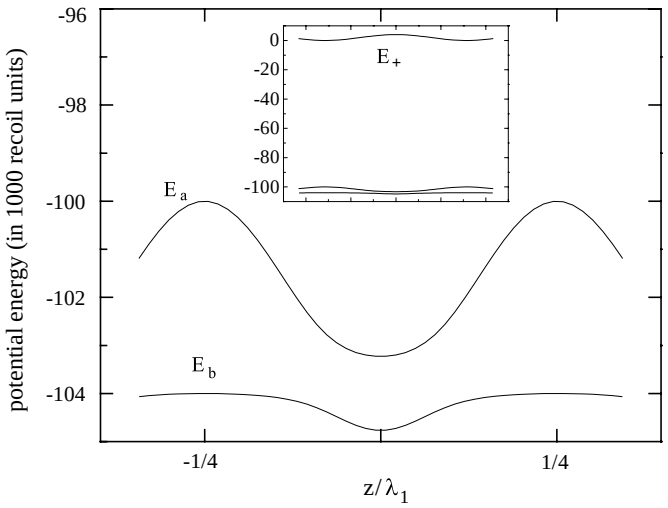

Fig. 16. The highly populated adiabatic potentials. The large plot shows the two strongly populated ones while the inset shows all three of them to illustrate their relative depths. The phase difference of the two standing waves is zero and the other parameters are as follows: $\Omega_1 = 40\Gamma_1$, $\Delta_1 = -100\Gamma_1$, $\Gamma_1 = 1000\,\omega_\mathrm{R}$; $\Omega_2 = 8\Gamma_2$, $\Delta_2 = -104\Gamma_2$, $\Gamma_2 = \Gamma_1$.

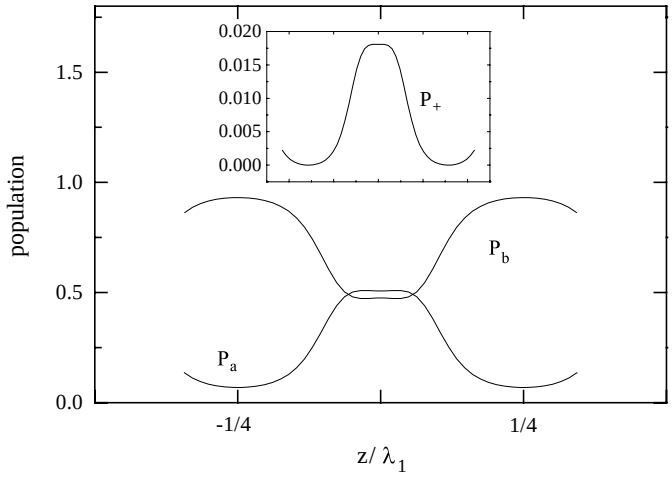

Fig. 17. The stationary population of the adiabatic potentials. The large plot shows the two mainly populated ones whereas the inset shows the population of the almost empty upper potential. The phase difference of the two standing waves is zero and the other parameters are the following: $\Omega_1 = 40\Gamma_1$, $\Delta_1 = -100\Gamma_1$, $\Gamma_1 = 1000\,\omega_\mathrm{R}$; $\Omega_2 = 8\Gamma_2$, $\Delta_2 = -104\Gamma_2$, $\Gamma_2 = \Gamma_1$.

5.2 Cooling scheme

As for the XV system the adiabatic potentials and their stationary populations suffice to provide a qualitative understanding of the motional aspects of the light matter interaction. We observe the anticipated dependence of

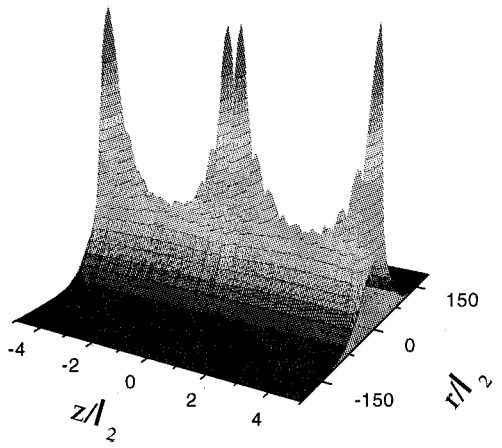

Fig. 18. Spatial distribution of the atoms over one period of the super-lattice. The z-axis is the direction of propagation of the two light fields. The parameters are $\Omega_1 = 40\Gamma_1,\ \Delta_1 = -100\Gamma_1,\ \Gamma_1 = 1000\,\omega_{\rm R};\ \Omega_2 = 8\Gamma_2,\ \Delta_2 = -104\Gamma_2,\ \Gamma_2 = \Gamma_1;\ k_2 = 0.9 \times k_1$. The FWHM of the light fields in radial direction is $140/k_1$. The explicit spatial dependence of the two standing waves is $\Omega_i(\mathbf{x}) = \Omega_i \sin(k_i z) \exp(-m_i(x^2 + y^2))$.

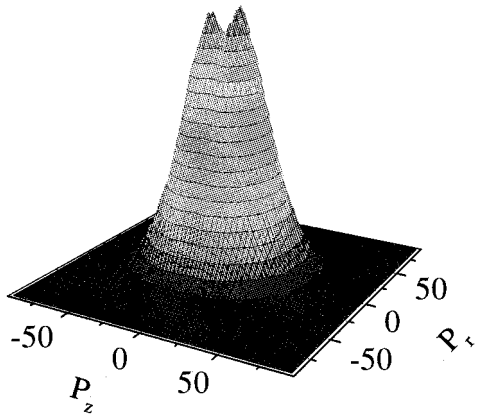

Fig. 19. Momentum distribution of the atoms. The z-axis is the direction of propagation of the two light fields. The parameters are $\Omega_1 = 40\Gamma_1,\ \Delta_1 = -100\Gamma_1,\ \Gamma_1 = 1000\,\omega_{\rm R};\ \Omega_2 = 8\Gamma_2,\ \Delta_2 = -104\Gamma_2,\ \Gamma_2 = \Gamma_1;\ k_2 = 0.9 \times k_1$. The FWHM of the light fields in radial direction is $140/k_1$.

the force on the relative phase of the two standing waves, which is, however, not as important as in the XV scheme. Figure 16 depicts the adiabatic potentials seen by a slowly moving atom, where the two light fields are in phase and have local maxima at $z = 0$. The small inset shows all of the three potentials while the main plot shows only the two strongly populated ones.

Figure 17 depicts the stationary population of the levels corresponding to the three adiabatic potentials. The main plot shows the populations of the lower two potentials E_a and E_b, while the inset depicts the population of the upper potential E_+. From this figure one can estimate the typical behavior of the atoms. They enter in the flat E_b-potential and roll down the sides of the small trough out of which they are preferably pumped into the steeper potential E_a. An escape out of E_a becomes more likely closer to the local maxima. In getting there they lose kinetic energy. Then they fall back to the flat potential again having lost kinetic energy in the process. In fact this process does not happen very often. A look at single trajectories shows that the atoms travel over many wavelengths staying on the E_b-potential before undergoing such a cooling cycle. Furthermore, in regions where the two light fields are far out of phase almost nothing happens because the amplitudes reach their maxima in regions where the effective detuning is much higher and so the pumping rates decrease.

5.3 Numerical results in 3D

As stated in the preceding section the atoms stay mainly on the E_b potential curve. This has the disadvantage that the relatively small gradient of this potential potential outside a region around the anti-nodes of the second light field strongly limits the trapping efficiency. To avoid this one can add a far–off-resonance trap, which only affects the level $|g_2\rangle$ and therefore mainly deforms the E_b potential. For the calculations leading to the results shown in Figures 18 and 19, we add a shallow trap in the following way. We assume that without the additional far red detuned laser the difference between E_b and E_a at the common nodes of the two standing waves would be only one third of what we want to have at $r = 0$. This is achieved by the following replacement:

$$E_b(z, r) \to E_b(z, r) + \frac{2}{3}(\Delta_1 - \Delta_2)(1 - e^{-m_3 r^2}),$$

where the radial dependence coefficient m_3 was chosen to be equal to m_1 and m_2, the radial coefficients of the Gaussian modes. Actually the detuning Δ_2 has to be regarded as the detuning between the σ_- polarised light field and the $|g_2\rangle - |e\rangle$ transition including the light shift of the $|g_2\rangle$ level induced by the additional far–off-resonant laser.

As one can see in Figures 18 and 19 there is localization and cooling and the atoms accumulate in the regions where the light fields both have their anti-nodes which is crucial for observing strong nonlinear cross-coupling effects. Note that there is a new double-peak structure in the momentum distribution, which appears due to the following reasons. The cooling is quite efficient only in a rather small region around the radial focus and atoms further away from the center see a light field configuration, which slightly heats in longitudinal direction. There the second light field is not resonantly coupled to the dressed state induced by the first one and the only remaining mechanical effect is dipole heating and diffusion both tending to expel atoms from the center of the momentum distribution.

6 Summary

We have demonstrated that using two TEM_{00} modes of an optical cavity, one gets a scheme which promises a

straightforward way to cool and trap atoms at the anti-nodes of a strong standing wave. The results have been obtained by semi-classical multi-potential propagation in 1D and 3D and were confirmed in 1D by Quantum Monte Carlo wave function simulations. Our setup generates cold and localized atoms, well suited for an investigation of nonlinear optical effects. Atoms initially within a disc of the diameter of the beam-waist and a thickness of the super-lattice period are strongly confined and trapped within a very few optical potential wells of the strong mode. The resulting high local atomic densities will of course be limited by atom-atom interactions. Furthermore, in the low density limit the system seems quite promising for studying intra-cavity QED effects with few atoms in the optical domain. Long interaction times and large cooperativities arise as a consequence of the atoms being trapped at the anti-nodes of the strong standing wave. Additional interesting effects should arise from an inclusion of the resonator dynamics [26].

Furthermore, for a Λ atom interacting with the two standing waves, it is possible to find a setup where the mechanical light effects strongly improve the nonlinear coupling between the two applied light fields.

We gratefully acknowledge stimulating discussions with J-F. Roch, J.-Ph. Poizat and Ph. Grangier. This work was supported by the Austrian Science Foundation under projects S6506-TEC (W.A. and K.M.G.) and S6504 (K.M.G.) and S6507-TEC (H.S. and K.E.). W.A. and K.M.G. acknowledge support from the ÖAD Amadeus programme under grant 4/96b and I.4. After completion of this work an experimental demonstration of a 3D bichromatic lattice at the university of Munich by Görlitz and Hänsch was brought to our attention.

Appendix A: Diagonalization of the Λ Hamiltonian

Appendix A gives some details of the analytical approximation used in the calculations for the eigenvalues and eigenstates of the local Hamiltonian. This is only shown for the Λ configuration, because the procedure for the V is basically the same.

In the bare basis $\{|e\rangle, |g_1\rangle, |g_2\rangle\}$ the internal Hamiltonian reads

$$\begin{pmatrix} 0 & \Omega_1/2 & \Omega_2/2 \\ \Omega_1/2 & \Delta_1 & 0 \\ \Omega_2/2 & 0 & \Delta_2 \end{pmatrix}.$$

By introducing $\cos 2\theta \equiv \Delta_1/\sqrt{\Omega_1^2+\Delta_1^2}$ and $\sin 2\theta \equiv \Omega_1/\sqrt{\Omega_1^2+\Delta_1^2}$ we diagonalize the upper left 2 by 2 block with the new basis $\{|+\rangle \equiv \sin\theta|e\rangle + \cos\theta|g_1\rangle, |-\rangle \equiv \cos\theta|e\rangle - \sin\theta|g_1\rangle, |g_2\rangle\}$. In our case $|g_2\rangle$ is nearly resonantly coupled to the $|-\rangle$ level. Hence we go on treating $|g_2\rangle$ and $|-\rangle$ as a driven two-level system which has no influence on the $|+\rangle$ state. With

$$\cos 2\phi \equiv \frac{\Delta_2 + \sqrt{\Omega_1^2+\Delta_1^2}\sin^2\theta}{E_2},$$

$$\sin 2\phi \equiv \frac{\Omega_2\cos\theta}{E_2},$$

$$E_2 \equiv \sqrt{(\Delta_2 + \sqrt{\Omega_1^2+\Delta_1^2}\sin^2\theta)^2 + \Omega_2^2\cos^2\theta},$$

we end up with the basis

$$|+\rangle \equiv \sin\theta|e\rangle + \cos\theta|g_1\rangle,$$

$$|a\rangle \equiv \sin\phi\cos\theta|e\rangle - \sin\phi\sin\theta|g_1\rangle + \cos\phi|g_2\rangle,$$

$$|b\rangle \equiv \cos\phi\cos\theta|e\rangle - \cos\phi\sin\theta|g_1\rangle - \sin\phi|g_2\rangle.$$

In this double-dressed basis the Hamiltonian reads

$$\begin{pmatrix} \sqrt{\Omega_1^2+\Delta^2}\cos^2\theta & \frac{\Omega_2}{2}\sin\theta\cos\phi & -\frac{\Omega_2}{2}\sin\theta\sin\phi \\ \frac{\Omega_2}{2}\sin\theta\cos\phi & \Delta_2 + E_2\sin^2\phi & 0 \\ -\frac{\Omega_2}{2}\sin\theta\sin\phi & 0 & \Delta_2 - E_2\cos^2\phi \end{pmatrix}.$$

Provided that Ω_1 is considerably larger than Ω_2, this is an excellent approximation to the result of a complete diagonalization of the Hamiltonian.

References

1. S. Chu, C. Wieman (Editors) *Laser Cooling and Trapping of Atoms*, J. Opt. Soc. Am. B (special issue) **6**, 2020 (1989).
2. E. Raab, M. Prantiss, A. Cable, S. Chu and D. Pritchard, Phys. Rev. Lett. **59**, 2631 (1987).
3. P. Bouyer *et al.*, Europhys. Lett. **59**, 2631 (1995).
4. H. Pu, T. Cai, N. P. Bigelow, T.T. Grove, P.L. Gould, Opt. Commun. **118**, 261 (1995).
5. K.M. Gheri, D.F. Walls, Phys. Rev. A **46**, R6793 (1992); K.M. Gheri, D. F. Walls, Phys. Rev. A **49**, 4134 (1994).
6. A. Lambrecht, T. Codreau, A.M. Steinberg, E. Giacobino, Europhys. Lett. **36**, 93 (1996).
7. J.-F. Roch, K. Vigneron, Ph. Grelu, A. Sinatra, J.-Ph. Poizat, Ph. Grangier, Phys. Rev. Lett. **78**, 634 (1997).
8. S. Stenholm, Rev. Mod. Phys. **58**, 699 (1986).
9. A.C. Doherty, A.S. Parkins, S.M. Tan, D.F. Walls, Phys. Rev. A **56**, 833 (1997).
10. W. Alge, K. Ellinger, H. Stecher, K.M. Gheri, H. Ritsch, Europhys. Lett. **39**, 491 (1997).
11. H. Mabuchi, Q.A. Turchette, M.S. Chapman, H.J. Kimble, Opt. Lett. **21**, 1393 (1996).
12. D.W. Vernooy, H.J. Kimble, Phys. Rev. A **56**, 4287 (1997).
13. S.H. Autler, C.H. Townes, Phys. Rev. **100**, 703 (1995).
14. J. Dalibard, C. Cohen-Tannoudji, J. Opt. Soc. Am. B **2**, 1707 (1985).
15. J.P. Gordon, A. Ashkin, Phys. Rev. **21**, 1606 (1980).
16. P. Marte, R. Dum, R. Taïeb, P. Zoller, Phys.Rev. A **47**, 4986 (1993).
17. C. Cohen-Tannoudji, in *Fundamental Systems in Quantum Optics*, Les Houches Session LIII (1990), edited by J. Dalibard, J.-M. Raimond, J. Zinn-Justin (North-Holland Elsevier Science, Amsterdam, 1992).

18. A. S. Parkins, P. Zoller, Phys. Rev. A **45**, 6522 (1992).
19. M. Drewsen, PhD Thesis, University of Århus(1993); M. Drewsen, Phys. Rev. A **51**, 1407 (1998).
20. Y. Castin, K. Berg-Sørensen, J. Dalibard, K. Mølmer, Phys. Rev. A **50**, 5092 (1994).
21. Y. Castin, J. Dalibard, C. Cohen-Tannoudji, in *Light Induced Kinetic Effects on Atoms, Ions and Molecules*, edited by L. Moi, S. Gozzini, C. Gabbanini, E. Arimondo, F. Strumia (ETS Editrice, Pisa, 1991) p. 5.
22. K.M. Gheri, PhD Thesis, University of Auckland (1993).
23. E. Bonderup, K. Mølmer, J. Opt. Soc. Am. B **6**, 2125 (1989).
24. R. Dum, P. Zoller, H. Ritsch, Phys. Rev. A **45**, 4879 (1992).
25. J. Dalibard, Y. Castin, K. Mølmer, Phys. Rev. Lett. **68**, 580 (1992).
26. P. Horak *et al.*, Phys. Rev. Lett. **79**, 4974 (1997).